VIP NMR Spectroscopy Very Important Paper

International Edition: DOI: 10.1002/anie.201903246
German Edition: DOI: 10.1002/ange.201903246

DNP-Supported Solid-State NMR Spectroscopy of Proteins Inside Mammalian Cells

Siddarth Narasimhan[+], Stephan Scherpe[+], Alessandra Lucini Paioni, Johan van der Zwan, Gert E. Folkers, Huib Ovaa, and Marc Baldus**

Abstract: *Elucidating at atomic level how proteins interact and are chemically modified in cells represents a leading frontier in structural biology. We have developed a tailored solid-state NMR spectroscopic approach that allows studying protein structure inside human cells at atomic level under high-sensitivity dynamic nuclear polarization (DNP) conditions. We demonstrate the method using ubiquitin (Ub), which is critically involved in cellular functioning. Our results pave the way for structural studies of larger proteins or protein complexes inside human cells, which have remained elusive to in-cell solution-state NMR spectroscopy due to molecular size limitations.*

Increasing evidence suggests that the highly complex and dynamic environment of the cell interior and its physiochemical setting imposes critical control on cellular functions, which is hardly reproducible under in vitro conditions. In-cell solution-state NMR spectroscopy can track such structural and dynamic interactions at the atomic level provided that proteins or other molecular units are small and tumble rapidly.[1–4] On the other hand, solid-state NMR spectroscopy (ssNMR) has been used to probe proteins and large protein complexes in bacterial cells[5–9] and at the cell membrane periphery of human cells.[10]

However, extending such studies to investigating proteins and molecular complexes inside human cells poses additional challenges. Firstly, molecule-specific isotope labeling must be achieved to spectroscopically detect the protein of interest in a complex cellular background. Furthermore, cellular ssNMR studies should be possible at endogeneous protein concentrations to ensure proper cell functioning. As a result, high-sensitivity ssNMR methods are needed that allow such proteins to be studied in an intact cellular environment. Dynamic nuclear polarization (DNP[11]), in which polarization is transferred from free electrons to atomic nuclei, greatly enhances ssNMR sensitivity. Previous work has shown that DNP is readily compatible with ssNMR on bacterial[7a] and human[10,12] cells, cell compartments[7–10,13] as well as cell lysates.[14,15] However, the strong reducing environment inside the cells can be deleterious to DNP radicals,[16] thus far precluding protein studies inside human cells.

Herein, we describe a dedicated ssNMR approach, detailed in Scheme 1, to overcome the aforementioned challenges by separating the biochemical and cell preparation steps from the NMR procedures, allowing us to directly examine molecular interactions inside cells at high-sensivity DNP conditions. In the first stage of Scheme 1, an isotope-labeled protein, prepared, for example, using recombinant expression in *Escherichia coli* or solid-phase peptide synthesis (SPPS, ref. [17]), is delivered into human cells of interest. In the current context, isotope-labeled protein was delivered into human cells by electroporation,[18] which, after a recovery period, can be followed by stage 2 in which cells are subjected to a stimulus or other functional treatments. Finally, and preceding the ssNMR measurements, DNP agents are introduced into the cells which are then filled into DNP-ssNMR magic angle spinning (MAS) rotors. At every stage,

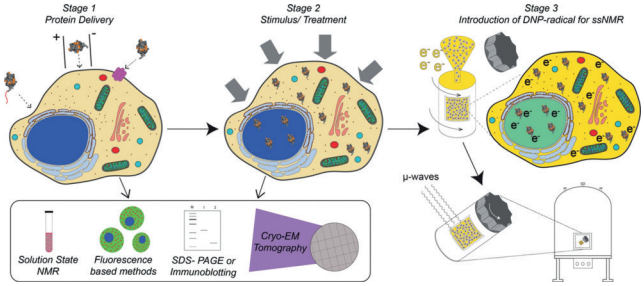

Scheme 1. In-cell DNP-supported solid-state NMR protocol. A general approach to studying molecular interactions inside human cells using DNP-supported ssNMR consisting of three steps, that is, isotope labeling and protein delivery, followed by applying a stimulus to the cells, and finally preparing the cells for DNP-ssNMR measurements using DNP agents (shown as electrons). Possible reference experiments, including solution-state NMR and microscopy studies utilized in the current work, are indicated.

[*] S. Narasimhan,[+] A. Lucini Paioni, J. van der Zwan, Dr. G. E. Folkers, Prof. Dr. M. Baldus
NMR Spectroscopy group, Bijvoet Center for Biomolecular Research, Utrecht University, Padualaan 8, 3584 CH Utrecht (The Netherlands)
E-mail: m.baldus@uu.nl

S. Scherpe,[+] Prof. Dr. H. Ovaa
Oncode Institute and Department of Cell and Chemical Biology, Leiden University Medical Center (LUMC)
Einthovenweg 20, 2333 ZC Leiden (The Netherlands)
E-mail: H.Ovaa@lumc.nl

[+] These authors contributed equally to this work.

Supporting information, including the Experimental Details (Section 3), and the ORCID identification number(s) for the author(s) of this article can be found under: https://doi.org/10.1002/anie.201903246.

biochemical and biophysical methods can be used to monitor cellular processes, thus paving the way for correlative studies including ssNMR.

To demonstrate the feasibility of the entire approach, we concentrated on ubiquitin (Ub), a post-translational modifier that regulates a large variety of cellular functions, particularly protein degradation.[19] The process known as ubiquitination entails the covalent attachment of Ub to the N-terminus or an internal lysine of a substrate, mediated by a concerted cascade of specialized classes of enzymes (E1, E2, and E3). Ub can itself be ubiquitinated in the same manner, leading to the formation of a variety of Ub chains that determine the fate of the substrate. While magnetic resonance studies of Ub have provided valuable insight into Ub chain formation in vitro (see, for example, Ref. [19a,20]), wild-type Ub has remained elusive to in-cell solution-state NMR[2] and previous studies have required the mutation of Ub residues known to be involved in numerous protein-protein interactions[2]. Using SPPS, we first introduced an N-terminal tetramethylrhodamine (TMR)-tag to the synthesized Ub (TMR–Ub). Confocal microscopy images of cells after recovery from electroporation (Figure 1A) revealed that the cells retained their

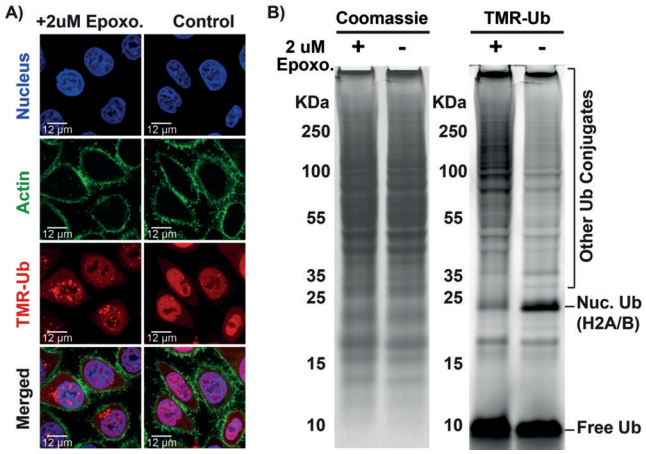

Figure 1. A) Single Z-slices of confocal microscopy images of electroporated TMR–Ub before (right) and after (left) proteasome inhibition. Note that in the latter case, the nuclear Ub pool is depleted and puncta-like formations are seen in the cytoplasm. B) SDS-PAGE (TMR scan) analysis of exogeneous TMR–Ub showing the formation of higher molecular weight conjugates and the depletion of nuclear Ub (25 KDa) upon proteasome inhibition.

normal morphology and that TMR–Ub was well integrated into the nuclear and cytoplasmic compartments. Importantly, electroporation enabled us to control the amount of protein delivered into cells, as evident from the presence of free monomeric and conjugated Ub at increasing concentrations on the western blot (Supporting Information, Figure S1A,C). Further analysis revealed that the concentration of Ub delivered into the cell is comparable to endogenous Ub concentrations[21] as seen from our western blots (Supporting Information, Figure S1B,D). Furthermore, an SDS-PAGE analysis using TMR–Ub allowed us to selectively track the exogenously introduced Ub population, which is, in addition to free monomeric Ub, mostly attached to 14–17 kDa proteins (Figure 1b), in line with earlier work[22] predicting Ub interactions with the nucleosomal proteins H2A and H2B. Indeed, such interactions would also be in line with the location of Ub in the nucleus as revealed by our confocal microscopy studies (Figure 1A). To further test the functionality of exogenous Ub, we performed a proteasome inhibition assay. The addition of the proteasome inhibitor epoxomicin led to the depletion of the nuclear Ub pool and an increase in the level of cytoplasmic Ub (Figure 1A, left), in line with earlier studies.[22] An increase in the levels of Ub conjugation to substrates was also apparent from western blotting against wild-type Ub (Supporting Information, Figure S1C,D) and SDS-PAGE (Figure 1B) probing exogeneous TMR–Ub. Taken together, these results suggested that exogenous Ub can be introduced into HeLa cells, and that it is functional as evident from conjugate formation in response to proteasome inhibition.

To check degradation of delivered Ub after electroporation and recovery, we conducted solution-state NMR experiments of ^{15}N-labeled wild-type Ub electroporated into HeLa cells (Figure 2). In line with earlier studies,[2,18] ^{15}N-^{1}H SOFAST-HMQC[23] experiments on cells suspended in Lei-

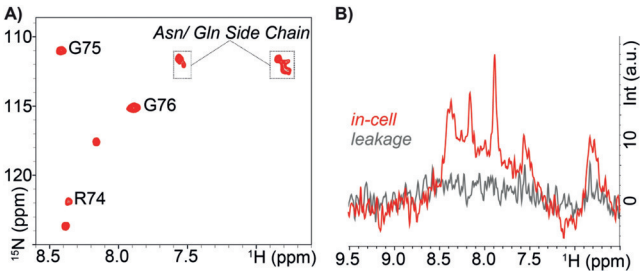

Figure 2. A) Solution-state NMR two-dimensional (^{1}H-^{15}N) SOFAST-HMQC spectra of ^{15}N-labeled Ub electroporated into HeLa cells performed 5 h after electroporation. Only backbone amide correlations emanating from the flexible C-terminal tail are detected, most likely from the free monoubiquitin pool. B) 1D slices were extracted from the spectra of in-cell ^{15}N-labeled Ub obtained before (red) and after (gray) depletion of the cells and showed negligible leakage of the protein during the NMR experiment.

bowitz L-15 medium revealed no traces of degradation. The spectrum (Figure 2A) contained five backbone amide correlations, of which R74, G75, and G76 in the C-Terminal tail were unambiguously identified. We confirmed that there was no protein leakage by recording a ^{15}N-edited ^{1}H 1D experiment on the medium (Figure 2B). In line with earlier work,[2] we attribute the absence of signals from the structured regions of Ub to the myriad of molecular recognition events and to the high viscosity of the cell interior. This notion was further confirmed by additional NMR experiments after cell-lysis in which the NMR signals of folded Ub were readily recovered without any sign of protein unfolding or degradation (Supporting Information, Figure S2). Most likely, the major population available to in-cell solution NMR studies is the free, unconjugated Ub, which constitutes only a fraction of the total Ub pool (Figure 1B and Supporting Information, Fig-

ure S1), further strengthening the need for ssNMR approaches.

For our ssNMR experiments described below, we estimated that 3.2 mm MAS rotors can hold about 5–8 million cells, corresponding to approximately 10–30 μg of labeled Ub in our ssNMR preparations (Supporting Information, Figure S3). Such quantities underline the need for efficient DNP for in-cell ssNMR studies. Previous calculations in our laboratory[24] have suggested that, to establish efficient DNP inside mammalian cells, the DNP agent must be localized inside the detached cells, for example as a result of rapid diffusion to minimize the effect of the reducing environment inside the cells. Using a DNP biradical variant of AMUPol[25] conjugated to TMR (Supporting Information, Figure S4) that was resuspended in a DNP buffer (see Section 3.9 of the Supporting Information), we tracked the location of DNP agents by confocal microscopy. Indeed, the water-soluble DNP agents were present in both nuclear and cytoplasmic cell compartments (Figure 3A) after a period of 10–15 minutes. Hence, we applied a similar time period in the final stage of our approach (Scheme 1) in which DNP-ssNMR MAS rotors were filled with cells using mild centrifugation. Subsequently, the DNP rotor was rapidly frozen in liquid nitrogen and transferred into the pre-cooled DNP-ssNMR probe.

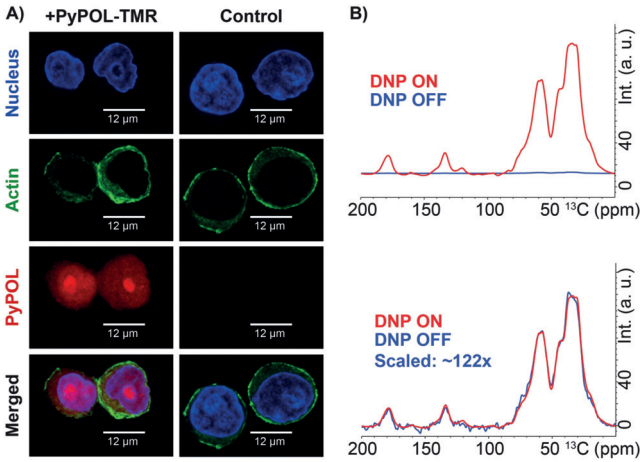

Figure 3. A) Z-Slices of confocal microscopy images showing that the radical (PyPOL-TMR, a variant of AMUPol) is well distributed in both nuclear and cytoplasmic compartments of the cell. B) DNP signal enhancement of approximately 122 times as seen on ^{1}H-^{13}C CP experiments under 400 MHz DNP conditions.

Using this procedure, we measured up to 130- and 35-times signal enhancement at 400 and 800 MHz DNP conditions (Figure 3B and Supporting Information, Figure S5), respectively, compared to the case without DNP. These results were significantly higher than previous studies on in situ systems, including human-cell vesicles[10] or fully labeled mammalian cells.[12] Moreover, ^{13}C T_1 relaxation times of protein signals ranged around 5 seconds further supporting the notion that the DNP agents were in close proximity to the target protein Ub.

These findings allowed us to conduct a series of 2D ssNMR experiments to detect Ub in our DNP-ssNMR preparations including double quantum-single quantum (2Q-1Q) ^{13}C,^{13}C and N to C_α (NCA) 2D experiments (Supporting Information, Figures S6 and S7). In Figure 4, the aliphatic region of a 2D ^{13}C, ^{13}C proton-driven spin

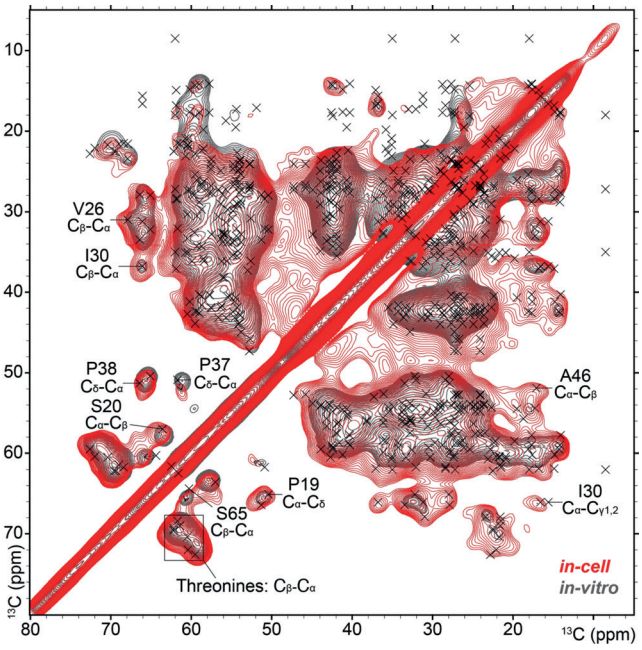

Figure 4. Aliphatic region of the 2D ^{13}C, ^{13}C-correlated PDSD experiment showing clear similarities in the spectrum of Ub in vitro (gray) and in cell (red). This confirms that UB remains folded after delivery into cells. This is further confirmed by our 3D DNP-ssNMR spectra. Indicated peaks were identified unambiguously.

diffusion (PDSD) experiment (see Figure S8 in the Supporting Information for the complete spectrum) is shown. For comparison, Figure 4 also includes results of a 2D DNP-ssNMR experiment on Ub before delivery into cells (black) in DNP buffer and in vitro NMR assignments of Ub at ambient temperature (black crosses, see Section 3.16 of the Supporting Information). Overall, the in vitro PDSD experiment was in good agreement with the in-cell ssNMR spectrum of Ub and included well-resolved correlations, such as for Ile30 and Pro37. To further improve spectral resolution, we resorted to 3D ssNMR (2Q-1Q-1Q) ^{13}C,^{13}C spectroscopy[26] (Figure 5 and Supporting Information, Figures S9–S12). Analysis of various 2D F_2,F_3 planes (Figure 5 and Supporting Information, Figures S9–S12) and F_1,F_3 planes (Supporting Information, Figures S9–S12) readily allowed us to unambiguously identify the chemical-shift correlations of Ub, including Lys63, which is a functional hotspot of polyubiquitination that is linked to regulatory functions other than proteasomal degradation. When plotted on the 3D structure of Ub, these residues for which correlations were identified unambiguously in the 2D and 3D experiments were located throughout the protein sequence, including the N-terminus as well as the five beta sheets and the central alpha helix (Figure 6).

With the combined analysis of 2D and 3D spectra, we could unambiguously trace back correlations (Supporting Information, Table ST1) for 25 residues, spread throughout

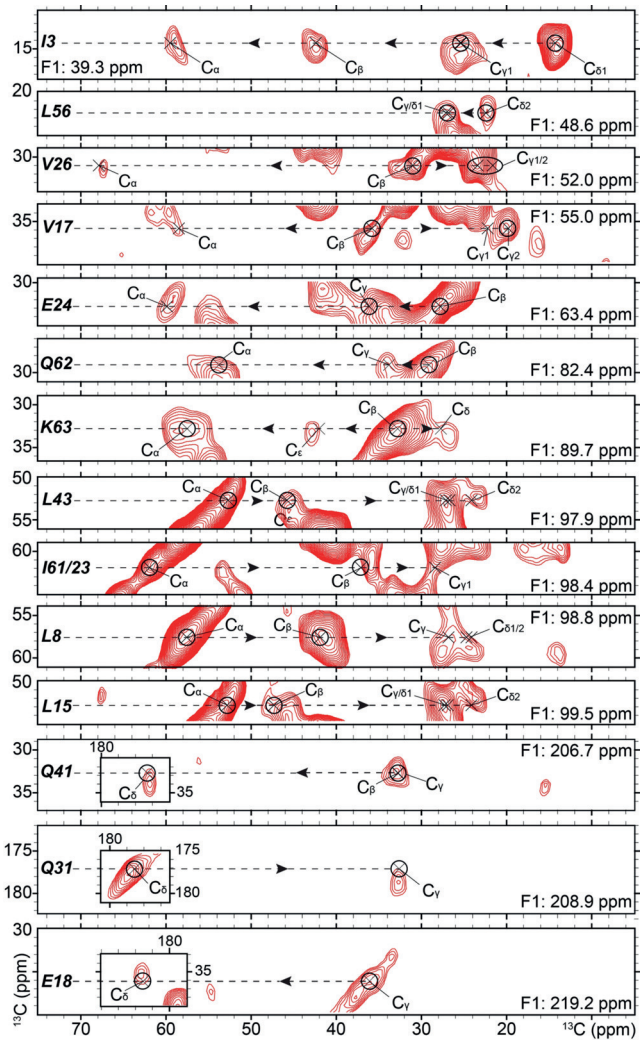

Figure 5. 2D (F2, F3) slices from the 3D (2Q-1Q-1Q) ^{13}C, ^{13}C spectrum corresponding to the unambiguously identifiable peaks. The F1 (2Q) frequency, indicated in the slices corresponds to the chemical shifts of encircled peaks.

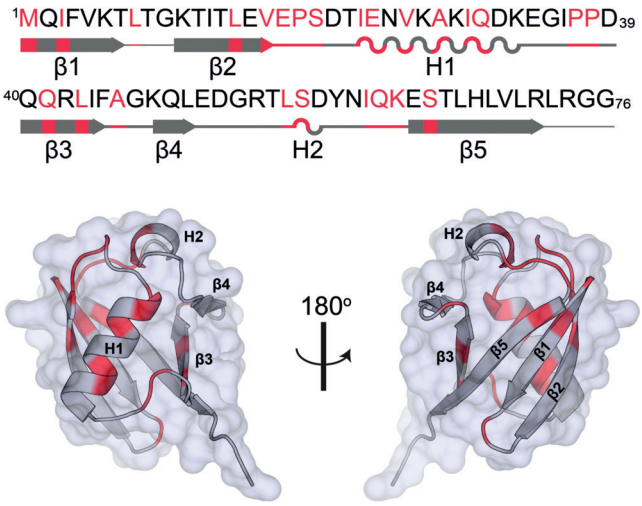

Figure 6. Residues of Ub for which correlations were identified unambiguously in the 2D and 3D experiments, plotted on the Ub crystal structure (PDB ID: 1UBQ) For further information, see the Supporting Information.

the protein, which matched with the in vitro assignments. This strongly suggests that uniformly [^{13}C,^{15}N]-labeled Ub remains folded after delivery into cells. Such a conclusion would also be consistent with our microscopy results and SDS-PAGE analysis in Figure 1, which confirmed the proper location and biological activity of our exogenously introduced Ub.

In summary, the presented in situ DNP-ssNMR scheme allowed us to detect Ub at endogeneous levels in human cells by NMR. To further increase spectral resolution, SPPS as well as tailored isotope-labeling, including amino-acid-specific forward or reverse labeling,[27] will be useful. For example, further studies that elucidate the effect of proteasomal inhibition by epoxomicin and other stress factors on Ub structures in cells are ongoing in our laboratory. Stress-induced polyubiquitination is followed by a plethora of molecular interactions within Ub chains.[19b,22] Uncovering the interactions between Ub molecules and specific interacting proteins in vivo is a long-term prospect for our work. By potentially co-introducing mixed-labeled[28] proteins (or other biomolecules), molecular interactions can be targeted and studied at atomic level in the cellular environment. Furthermore, such experiments could be readily extended to other Ub-like proteins, such as SUMO or NEDD8.[19b]

In the current context, we have used electroporation, which has successfully been used for the delivery of proteins (see, for example, Ref. [18]) or nucleic acids into cells. In cases where this technique is not suited, for example due to protein size or solubilization issues, the present approach could be combined with other delivery methods (Scheme 1), such as cell-penetrating peptides (CPP[2]), pore-forming toxins,[29] or directed protein expression,[4] to achieve molecule-specific labeling in the cells of interest. Likewise, our method complements advanced microscopy, such as confocal microscopy, used in the present study, or electron tomography,[6c] studies to obtain unprecedented insights from the atomic to the nanometer level on molecular interactions and modifications that take place inside human cells. Such studies could significantly expand our understanding of cellular processes ranging from protein synthesis, folding, and clearance to cellular signaling.

Acknowledgements

We are indebted to Professor Paul Tordo and Dr. Olivier Ouari (Aix-Marseille Université, Marseille) for providing AMUpol and PyPol-MTSSL. We thank Mark Daniëls for technical support as well as helpful discussions, along with Suzan Leemans for the latter. We thank Hugo van Ingen and Rolf Boelens for providing access to the 900 MHz solution-state NMR instrument. We are grateful to Dr. Philipp Selenko and his group (Weizmann Institute) for sharing their expertise with protein delivery into eukaryotic cells using electroporation. This work was funded in part by the Netherlands Organisation for Scientific Research (NWO) (Graduate Program; project 022.005.029, Netherlands' Magnetic Reso-

nance Research School, NMARRS, a VICI grant to H.O. as well as grants 700.26.121 and 700.10.443 to M.B.) and iNEXT (project number 653706), a Horizon 2020 program of the European Union.

Conflict of interest

The authors declare no conflict of interest.

Keywords: dynamic nuclear polarization · in-cell NMR · protein–protein interactions · solid-state NMR · ubiquitination

How to cite: *Angew. Chem. Int. Ed.* **2019**, *58*, 12969–12973
Angew. Chem. **2019**, *131*, 13103–13107

[1] C. Li, J. Zhao, K. Cheng, Y. Ge, Q. Wu, Y. Ye, G. Xu, Z. Zhang, W. Zheng, X. Zhang, X. Zhou, G. Pielak, M. Liu, *Annu. Rev. Anal. Chem.* **2017**, *10*, 157–182.
[2] K. Inomata, A. Ohno, H. Tochio, S. Isogai, T. Tenno, I. Nakase, T. Takeuchi, S. Futaki, Y. Ito, H. Hiroaki, M. Shirakawa, *Nature* **2009**, *458*, 106–109.
[3] R. Hänsel, L. M. Luh, I. Corbeski, L. Trantirek, V. Dötsch, *Angew. Chem. Int. Ed.* **2014**, *53*, 10300–10314; *Angew. Chem.* **2014**, *126*, 10466–10480.
[4] E. Luchinat, L. Banci, *Acc. Chem. Res.* **2018**, *51*, 1550–1557.
[5] S. Reckel, J. J. Lopez, F. Löhr, C. Glaubitz, V. Dötsch, *ChemBioChem* **2012**, *13*, 534–537.
[6] a) M. Renault, R. Tommassen-van Boxtel, M. P. Bos, J. A. Post, J. Tommassen, M. Baldus, *Proc. Natl. Acad. Sci. USA* **2012**, *109*, 4863–4868; b) M. E. Ward, S. Wang, R. Munro, E. Ritz, I. Hung, P. L. Gor'kov, Y. Jiang, H. Liang, L. S. Brown, V. Ladizhansky, *Biophys. J.* **2015**, *108*, 1683–1696; c) L. A. Baker, T. Sinnige, P. Schellenberger, J. de Keyzer, C. A. Siebert, A. J. M. Driessen, M. Baldus, K. Grunewald, *Structure* **2018**, *26*, 161–170.
[7] a) M. Renault, S. Pawsey, M. P. Bos, E. J. Koers, D. Nand, R. Tommassen-van Boxtel, M. Rosay, J. Tommassen, W. E. Maas, M. Baldus, *Angew. Chem. Int. Ed.* **2012**, *51*, 2998–3001; *Angew. Chem.* **2012**, *124*, 3053–3056; b) T. Jacso, W. T. Franks, H. Rose, U. Fink, J. Broecker, S. Keller, H. Oschkinat, B. Reif, *Angew. Chem. Int. Ed.* **2012**, *51*, 432–435; *Angew. Chem.* **2012**, *124*, 447–450.
[8] M. Kaplan, A. Cukkemane, G. C. P. van Zundert, S. Narasimhan, M. Daniels, D. Mance, G. Waksman, A. Bonvin, R. Fronzes, G. E. Folkers, M. Baldus, *Nat. Methods* **2015**, *12*, 649–652.
[9] K. Yamamoto, M. A. Caporini, S.-C. Im, L. Waskell, A. Ramamoorthy, *Biochim. Biophys. Acta Biomembr.* **2015**, *1848*, 342–349.
[10] M. Kaplan, S. Narasimhan, C. de Heus, D. Mance, S. van Doorn, K. Houben, D. Popov-Celeketic, R. Damman, E. A. Katrukha, P. Jain, W. J. C. Geerts, A. J. R. Heck, G. E. Folkers, L. C. Kapitein, S. Lemeer, P. Henegouwen, M. Baldus, *Cell* **2016**, *167*, 1241–1251.
[11] Q. Z. Ni, E. Daviso, T. V. Can, E. Markhasin, S. K. Jawla, T. M. Swager, R. J. Temkin, J. Herzfeld, R. G. Griffin, *Acc. Chem. Res.* **2013**, *46*, 1933–1941.
[12] B. J. Albert, C. Gao, E. L. Sesti, E. P. Saliba, N. Alaniva, F. J. Scott, S. T. Sigurdsson, A. B. Barnes, *Biochemistry* **2018**, *57*, 4741–4746.
[13] J. Medeiros-Silva, S. Jekhmane, A. Lucini Paioni, K. Gawarecka, M. Baldus, E. Swiezewska, E. Breukink, M. Weingarth, *Nat. Commun.* **2018**, *9*, 3963.
[14] K. K. Frederick, V. K. Michaelis, B. Corzilius, T.-C. Ong, A. C. Jacavone, R. G. Griffin, S. Lindquist, *Cell* **2015**, *163*, 620–628.
[15] T. Viennet, A. Viegas, A. Kuepper, S. Arens, V. Gelev, O. Petrov, T. N. Grossmann, H. Heise, M. Etzkorn, *Angew. Chem. Int. Ed.* **2016**, *55*, 10746–10750; *Angew. Chem.* **2016**, *128*, 10904–10908.
[16] I. Krstić, R. Hänsel, O. Romainczyk, J. W. Engels, V. Dötsch, T. F. Prisner, *Angew. Chem. Int. Ed.* **2011**, *50*, 5070–5074; *Angew. Chem.* **2011**, *123*, 5176–5180.
[17] F. El Oualid, R. Merkx, R. Ekkebus, D. S. Hameed, J. J. Smit, A. de Jong, H. Hilkmann, T. K. Sixma, H. Ovaa, *Angew. Chem. Int. Ed.* **2010**, *49*, 10149–10153; *Angew. Chem.* **2010**, *122*, 10347–10351.
[18] F.-X. Theillet, A. Binolfi, B. Bekei, A. Martorana, H. M. Rose, M. Stuiver, S. Verzini, D. Lorenz, M. van Rossum, D. Goldfarb, P. Selenko, *Nature* **2016**, *530*, 45–50.
[19] a) C. M. Pickart, D. Fushman, *Curr. Opin. Chem. Biol.* **2004**, *8*, 610–616; b) K. N. Swatek, D. Komander, *Cell Res.* **2016**, *26*, 399–422.
[20] A. Kniss, D. Schuetz, S. Kazemi, L. Pluska, P. E. Spindler, V. V. Rogov, K. Husnjak, I. Dikic, P. Güntert, T. Sommer, T. F. Prisner, V. Dötsch, *Structure* **2018**, *26*, 249–258.
[21] S. E. Kaiser, B. E. Riley, T. A. Shaler, R. S. Trevino, C. H. Becker, H. Schulman, R. R. Kopito, *Nat. Methods* **2011**, *8*, 691–696.
[22] N. P. Dantuma, T. A. M. Groothuis, F. A. Salomons, J. Neefjes, *J. Cell Biol.* **2006**, *173*, 19–26.
[23] P. Schanda, Ē. Kupče, B. Brutscher, *J. Biomol. NMR* **2005**, *33*, 199–211.
[24] D. Mance, M. Weingarth, M. Baldus in *Modern Magnetic Resonance* (Ed.: G. A. Webb), Springer International Publishing, Cham, **2018**, pp. 487–503.
[25] a) C. Sauvée, M. Rosay, G. Casano, F. Aussenac, R. T. Weber, O. Ouari, P. Tordo, *Angew. Chem. Int. Ed.* **2013**, *52*, 10858–10861; *Angew. Chem.* **2013**, *125*, 11058–11061; b) E. A. W. van der Cruijsen, E. J. Koers, C. Sauvee, R. E. Hulse, M. Weingarth, O. Ouari, E. Perozo, P. Tordo, M. Baldus, *Chem. Eur. J.* **2015**, *21*, 12971–12977.
[26] H. Heise, K. Seidel, M. Etzkorn, S. Becker, M. Baldus, *J. Magn. Reson.* **2005**, *173*, 64–74.
[27] M. Renault, A. Cukkemane, M. Baldus, *Angew. Chem. Int. Ed.* **2010**, *49*, 8346–8357; *Angew. Chem.* **2010**, *122*, 8524–8535.
[28] M. Weingarth, M. Baldus, *Acc. Chem. Res.* **2013**, *46*, 2037–2046.
[29] S. Ogino, S. Kubo, R. Umemoto, S. Huang, N. Nishida, I. Shimada, *J. Am. Chem. Soc.* **2009**, *131*, 10834–10835.

Manuscript received: March 15, 2019
Accepted manuscript online: June 24, 2019
Version of record online: July 19, 2019

